Cellulose (2016) 23:1825–1846
DOI 10.1007/s10570-016-0912-3

ORIGINAL PAPER

A comparative guide to controlled hydrophobization of cellulose nanocrystals via surface esterification

Shane X. Peng · Huibin Chang · Satish Kumar · Robert J. Moon · Jeffrey P. Youngblood

Received: 27 August 2015 / Accepted: 12 March 2016 / Published online: 19 March 2016

Abstract Surface esterification methods of cellulose nanocrystals (CNC) using acid anhydrides, acid chlorides, acid catalyzed carboxylic acids, and 1′1-carbonyldiimidazole (CDI) activated carboxylic acids were evaluated with acetyl-, hexanoyl-, dodecanoyl-, oleoyl-, and methacryloyl-functionalization. Their grafting efficiency was investigated using Fourier-transform infrared spectroscopy and ^{13}C solid state NMR spectroscopy. Acid anhydride and CDI were found to be the most applicable reagents to graft short and long chain aliphatic carbons, respectively. The preservation of structural morphology and crystallinity of grafted CNCs were confirmed using transmission electron microscopy and X-ray diffraction. The hydrophobicity of grafted CNCs was evaluated by dispersing them in organic solvents with different Hansen's solubility parameters. The dispersibility of grafted CNCs in organic solvents was improved by using never-dried CNCs as source materials and keep CNCs wet in their washing solvents after grafting, thus increasing the solvency range to disperse CNCs.

Keywords Cellulose nanocrystals · Esterification · Hydrophobicity · Hansen's solubility parameters · Dispersibility

Electronic supplementary material The online version of this article (doi:10.1007/s10570-016-0912-3) contains supplementary material, which is available to authorized users.

S. X. Peng · R. J. Moon · J. P. Youngblood (✉)
School of Materials Engineering, Purdue University, West Lafayette, IN 47907, USA
e-mail: jpyoungb@purdue.edu

H. Chang · S. Kumar
School of Materials Science and Engineering, Georgia Institute of Technology, Atlanta, GA 30332, USA

H. Chang · S. Kumar
Renewable Bioproducts Institute, Georgia Institute of Technology, Atlanta, GA 30332, USA

R. J. Moon
Forest Products Laboratory, USDA Forest Service, Madison, WI 53726, USA

Introduction

Nanotechnology research has always been a tug of war of improving performance and properties versus reducing cost and environmental impact. Cellulose nanomaterials (CNs) possess the best of both worlds with their unique set of mechanical, thermal, and optical properties as well as their inherent sustainability and abundancy (Hobbs et al. 1998; Moon et al. 2011; Reising et al. 2012; Diaz et al. 2013, 2014). CNs are nanoparticles consisting of cellulose and are extracted from biomass such as trees, plants, bacteria, and algae (Beck-Candanedo et al. 2005). Among many types of CNs, cellulose nanocrystals (CNCs) have received increasing attention. CNCs are whisker

or rod shaped CNs obtained from acid hydrolysis with high aspect ratio (3–10 nm wide and 50–500 nm long), high crystallinity, low density, and low coefficient of thermal expansion (Elazzouzi-Hafraoui et al. 2008; Park et al. 2010; Diaz et al. 2013). Applications for CNCs have been found in nanocomposites, organic electronics, laminates, fibers, cements, and biomaterials (Zhou et al. 2013; Chen et al. 2014; Liu et al. 2014; Peng et al. 2014; Cao et al. 2015; Liu et al. 2015). While applications for CNCs have been expanding, one of the challenges of utilizing CNCs is to overcome their surface hydrophilicity. The surface of CNC is covered with the hydroxyl groups from the anhydroglucose repeating units of cellulose. This chemical configuration has led to interfacial incompatibilities and low dispersibility of CNCs in hydrophobic media and matrices. A variety of processing strategies have been taken toward alleviating this incompatibility issue including solvent exchange and composite design (Capadona et al. 2007; Liu et al. 2014; Peng et al. 2014). Nonetheless, applications such as polymer melt processing require fundamental change to the surface properties of CNCs. Therefore, surface modification becomes the necessary approach to increase surface hydrophobicity of CNCs.

Similar to other nanoparticles and polymeric materials, surface modification of CNCs can be achieved through either physical adsorption or chemical grafting (Missoum et al. 2013; Habibi 2014). The adsorption approach typically utilizes surfactants or polyelectrolytes, which rely on electrostatic interactions and have potential migration issues of adsorbed moieties (Heux et al. 2000; Podsiadlo et al. 2005). The chemical grafting approach generates covalent linkages between CNC and the grafted moieties. Both small molecules and macromolecules can be semi-irreversibly attached with this approach. A wide variety of chemical reactions can be utilized to modify the surface hydroxyl groups of CNC including oxidation (Isogai et al. 2011), carbamation (Habibi and Dufresne 2008; Siqueira et al. 2009), etherification (Dong and Roman 2007; Hasani et al. 2008), and esterification. Among these reactions, esterification is most of common method chosen for its simplicity and versatility (Eyley and Thielemans 2014). In general, esterification reaction can be categorized into five different groups based on the reagents and catalysts used: acid halides, acid anhydrides, acid catalyzed carboxylic acids, transesterification esters, and in situ activated carboxylic acids with the most popular being the utilization of acid halides (Morandi et al. 2009; Berlioz et al. 2009; Junior de Menezes et al. 2009; Majoinen et al. 2011; Fumagalli et al. 2013; Bendahou et al. 2014; Navarro et al. 2015). For this reaction, the carbonyl group on the acid chloride or acid bromide is attacked by the hydroxyl groups of CNCs and produces HCl or HBr as byproduct. Typically, a base such as pyridine or triethylamine is used to neutralize the HCl or HBr generated. Another popular method is the utilization of acid anhydrides (Sassi and Chanzy 1995; Cetin et al. 2009; Lin et al. 2011; Missoum et al. 2012) or succinic anhydride (Yuan et al. 2006). In the case of acid anhydrides, additional catalysts such as pyridine are typically added to speed the reaction. For acid catalyzed esterification of CNCs using carboxylic acid, the mechanism is the classic Fischer esterification reaction, where the carbonyl group on the carboxylic acid is activated with a strong acid (Espino-Pérez et al. 2014). This method requires carboxylic acids that are soluble in protic solvents. A similar reaction can also be performed during the acid hydrolysis stage of the CNC production (Braun and Dorgan 2009; Braun et al. 2012; Boujemaoui et al. 2015). Transesterification is another popular method used to modify CNCs. Typically, the reaction coincides with the ring-opening polymerization of the reagents, where long chain polymers can be grafted from CNCs surface and acid or organometallic compounds are used as catalysts (Labet and Thielemans 2011, 2012; Xiao et al. 2012; Tian et al. 2014; Gårdebjer et al. 2015). In recent years, more interest has been drawn toward the use of coupling agents to modify cellulosic materials with carboxylic acids (Heinze et al. 2006). The most common coupling agents including 1′1-carbonyldiimidazole (CDI) (Araki and Mishima 2014), carbodiimide (Nielsen et al. 2010), and 4-toluenesulfonyl chloride (TsCl) (Lee et al. 2011; Sadeghifar et al. 2011; Lee and Bismarck 2012; Jasmani et al. 2013; Lin and Dufresne 2014). Despite having different reaction mechanisms, these reagents feature the ability to activate the otherwise less reactive carboxylic acids in a one-pot reaction.

Although the current research literature presents a large database of esterification method, it is yet challenging to select the most viable and application specific method to hydrophobize CNCs. Reaction efficiency of the methods used in literature is often

difficult to compare due to differences in CNC source material, structure of grafted molecule, reactivity of the reagents, and characterization and degree of substitution calculation method used. The surface chemistry of the starting CNC materials also varies depending on the acid hydrolysis processing conditions (Beck-Candanedo et al. 2005). Sulfuric acids hydrolyzed CNC has various amounts of sulfate half-esters while hydrochloric acid treated CNC does not (Araki et al. 1998). In addition, the objective and application of each esterification study varies. Often depending on the applications, the degree of hydrophobicity of modified CNCs needs to be controlled. Therefore, there is a necessity for a goal-oriented study that compares and contrasts the different esterification methods with respect to the different types of functional groups grafted.

In this study, a comparative study of CNC esterification methods with the focus on controlling the hydrophobicity of CNCs was conducted. Esterification using acid chloride, acid anhydride, acid catalyzed carboxylic acid, and in situ activated carboxylic acid were performed. Wood derived CNCs were grafted with different length of hydrocarbons utilizing these methods. To our knowledge, this is the first cross-comparison study of different CNC esterification methods using CNCs from the same source material. In addition, the effect of freeze-drying versus solvent exchange processing before and after the reactions were also evaluated in order to further improve the hydrophobicity of the grafted CNCs. Dispersibility studies were used to assess the relative hydrophobicity range of the grafted CNCs. An alternative approach and mechanism on dispersing grafted CNCs in hydrophobic solvent was also proposed.

Experimental section

Materials

Dimethyl sulfoxide (DMSO, anhydrous 99.9 %), pyridine (anhydrous 99.8 %), tetrahydrofuran (THF, anhydrous 99.9 %, inhibitor-free), *N,N*-dimethylforamide (DMF, anhydrous 99.8 %), triethylamine (TEA, 99 %), 1′1-carbonyldiimidazole (CDI, reagent grade), acetone (ACS reagent), hydrochloric acid (ACS reagent 37 %), cyclohexane (99.7 %), hexane (anhydrous 95 %), and the reagents listed in Table S1 in the Supplementary Information were purchased from Sigma Aldrich, St. Louis, MO, USA. Methanol (anhydrous 99.8 %) and Ethanol (200 proof) were purchased from VWR, West Chester, PA, USA. All reagents were used as received without further purification. Freeze-dried CNCs (FD) and 11.9 wt% never-dried CNC suspension in water (ND) were provided by USDA Forest Service-Forest Products Laboratory (FPL), Madison, WI, USA.(Reiner and Rudie 2013) Both FD and ND are in sulfate half-ester form with 0.96 and 1 wt% sulfur, respectively and have sodium as counter ion.

Esterification of CNCs

Four esterification routes were utilized to graft five different side groups to CNCs. Reaction conditions were selected according to best results as reported from literature. The schematic of the reactions is illustrated in Fig. 1. Acetyl, hexanoyl, and dodecanoyl grafted CNCs were synthesized using all four esterification routes, while Methacryloyl and oleoyl grafted CNCs were synthesized using routes 2 and 3, respectively. FDs were used as starting materials for routes 1–3, while NDs were used for route 4. In addition, dodecanoyl and oleoyl were grafted on to both FDs and NDs using route 3. The accessible surface hydroxyl groups of CNCs used in this study were calculated to be 2.74 mmol/g for FD and 3.18 mmol/g for ND via method introduced by Eyley and Thielemans (2014). Detail calculation is elaborated in the Supplementary Information.

Dispersion of CNCs in reaction solvents

For synthesis route 1, 1 g of dried FDs were initially dispersed in 20 mL DMSO using a sonifier (S-250D, Branson Ultrasonics Corp., Danbury, CT, USA) at 40 % amplitude and 1-s on/off cycles until transparent suspensions were obtained. DMSO/CNC suspension was first solvent exchanged with THF via consecutive dispersion–centrifugation steps. Four times volume excess of THF was mixed with DMSO/CNC suspensions using a vortexer (VWR, West Chester, PA, USA). The mixture was centrifuged (VWR Clinical 200) at 4000*g* for 15 min. The supernatant was replaced with fresh THF and the CNCs were redispersed using the vortexer. This dispersion–centrifugation procedure was performed four times. The

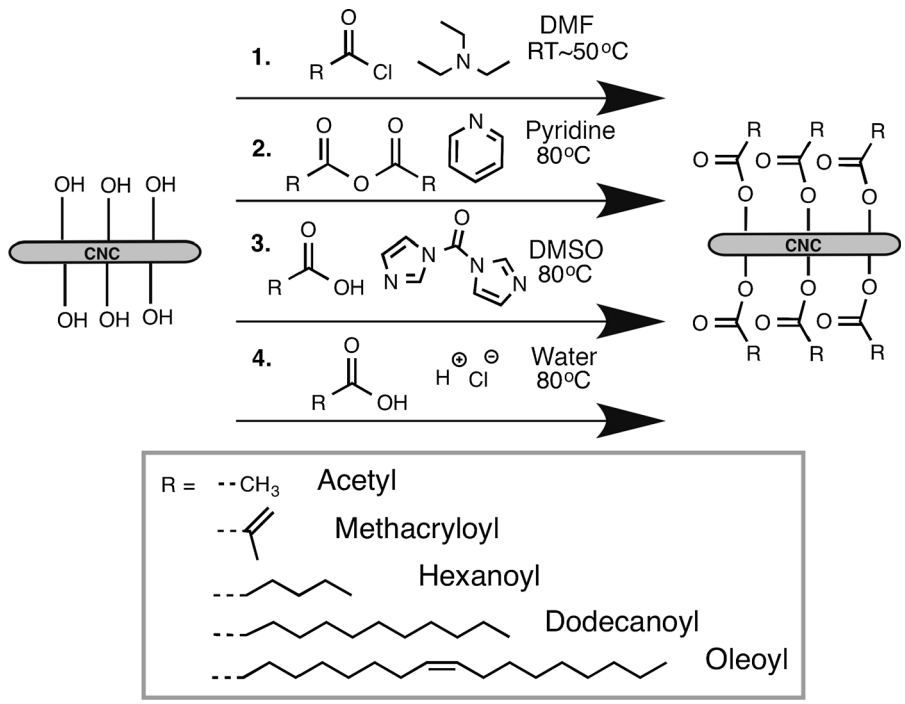

Fig. 1 Synthesis routes of CNC esterification reactions that were conducted in parallel using acid chlorides (*route 1*), acid anhydrides (*route 2*), CDI activated carboxylic acids (*route 3*), and acid catalyzed carboxylic acids (*route 4*)

reason behind this process was that both DMSO an DMF were good solvent for CNC, therefore it was difficult to completely remove DMSO from DMF by direct solvent exchange. At the end of this solvent exchange process, CNCs were redispersed in DMF with a vortexer. Residual THF was removed via rotary evaporator. For route 2, FDs were first dispersed in DMSO using a sonifier, then directly solvent exchanged with pyridine six times following similar procedure as route 1. CNCs were redispersed in excess pyridine after solvent exchange. For route 3, both FDs and NDs were used. The FDs were dispersed in DMSO using a sonifier, while the ND suspension was first solvent exchanged with acetone six times and redispersed in DMSO. Residual acetone was removed via rotary evaporator. For route 4, ND suspension was directly added to fatty acids regents without additional dispersion steps.

Synthesis routes for CNC esterification reactions

Synthesis route 1 was based on method developed by Thielemans et al. (2006). The reactions were conducted in a necked round-bottomed flask with magnetic stirring. CNC/DMF suspension was first added to the flask. TEA was added as HCl trap. Acid chloride reagent was added drop-wise to initiate the reaction. An ice bath was used during acetyl chloride addition. After reagent addition, temperature was raised to the corresponding reaction temperatures listed in Table S1. N_2 gas flow was introduced to remove evolved HCl gas.

Synthesis route 2 was based on the method developed by Lin et al. (2011). However, FD was dispersed in pyridine via solvent exchange instead of ultrasonication. CNC/pyridine suspension was added in a three-necked round-bottomed flask equipped with a condenser with magnetic stirring. For the methacryloyl grafting reaction, CNC/pyridine suspension was bubbled with N_2 gas overnight before the addition of the reagent. The grafting reaction was conducted under N_2 atmosphere to prevent crosslinking and side reactions.

Synthesis route 3 was based on CDI mediated method developed for cellulose by Hussain et al. (2004). Reaction was conducted in a three-necked round-bottomed flask equipped with a condenser under magnetic stirring. CDI were first dissolved in DMSO and mixed with equal molar ratio of carboxylic

acid reagents. The mixture was stirred overnight at 60 °C with N_2 gas flow to remove evolved CO_2. Afterwards, CNC/DMSO suspension produced from either FD or ND starting materials was added to the mixture to initiate the reaction. Afterwards, temperature was raised to the corresponding reaction temperatures listed in Table S1.

Synthesis route 4 was based on a method developed by Espino-Pérez et al. (2014). ND suspension in water was added to a distillation system in order to constantly remove water. 5 % molar equivalent of HCl was added to reaction flask. Reagents were added at temperature above their melting point. Detailed experimental conditions for all synthesis routes are listed in the Supplementary Information Table S1.

Extraction and purification of grafted CNCs

At the end of each reaction, the grafted CNCs were precipitated from large excess of the designated washing solvent listed in Table S1 in the Supplementary Information. The products were purified by consecutive dispersion–centrifuge steps described in "Dispersion of CNCs in reaction solvents" section (4000*g* for 15 min) to remove residual reactants. As suggested by other researchers, the dispersion–centrifuge method of purification was better suited for nanoscale objects as it prevented excess sample lost and had similar efficiency to Soxhlet extraction (Siqueira et al. 2010; Espino-Pérez et al. 2014). Grafted CNCs were either freeze-dried using a lyophilizer (Labconco FreeZone Plus 4.5L) or kept in their respective washing solvents.

Characterization

Fourier transform infrared spectroscopy (FT-IR)

FT-IR spectra of unmodified and grafted CNCs were obtained by making KBr pellets of the samples and tested in transmission mode (FTIR Spectrum 100, PerkinElmer, Waltham, MA, USA). Ten scans were taken per sample range from 450 to 4000 cm^{-1} with a resolution of 4 cm^{-1}.

^{13}C CP-MAS solid-state NMR spectroscopy

^{13}C CP-MAS spectra were obtained on a Chemagnetics CMX-400 NMR spectrometer equipped with a wide-bore magnet and a 5 mm triple-resonance (H–X–Y) MAS probe. The pulse sequence used was the "cp_toss_pm" sequence from the spectrometer's pulse program library, which includes the TOSS (Dixon et al. 1982) and TPPM techniques. Acquisition parameters included ^{1}H and ^{13}C RF field strengths of 50 kHz, a cross-polarization time of 2 ms, a TPPM decoupling pulse of 7.1 μs, a relaxation delay of 6 s, a data acquisition time of 32 ms with a sweep width of 32 kHz, and a sample spinning rate of 5.6 kHz. Typically, 1024–2048 scans were acquired (103–206 min) and the data were processed with exponential multiplication (line-broadening of 35 Hz) and zero-filled twice prior to Fourier transformation.

Elemental analysis

To support the solid-state NMR results and check for impurities, elemental Analysis was conducted by Galbraith Laboratories (Knoxville, TN, USA). Carbon, hydrogen, and oxygen contents were measured for FD CNC and grafted CNCs using different methods. The tests were performed twice and the average was used. The degree of substitution was calculated following the method proposed by Vaca-Garcia et al. (2001)

X-ray diffraction analysis (XRD)

Unmodified CNC and grafted CNC powder were pressed into pellets and mounted on adhesive tapes. They were evaluated in a Bruker GADDS 2D X-ray diffractometer using a 546 nm Cu Kα source at 30 mA, 10 kV for 360 s and a beam size of 500 μm at 6.13 cm from detector in transmission mode. The crystallinity, X_c, of unmodified CNC and grafted CNC was calculated Eq. (1) (Park et al. 2010).

$$X_c(\%) = \left(\frac{A_c}{A_c + A_a}\right) \times 100 \quad (1)$$

where A_c and A_a represents the total crystalline and amorphous area, respectively, of deconvoluted XRD patterns. The XRD deconvolution was completed with MDI Jade 8.5.2 software in which the measured XRD pattern was fitted using peak assignments based on idealized powder diffraction patterns of cellulose I and II (French 2014) and peak shape profiles were assumed to be pseudo-Voigt. Next, a refinement method was used to minimize differences between the fitted XRD

pattern and the measured pattern (Rietveld 1969; Hamad and Hu 2010). Note that CNC from the FPL process consist of both Cellulose I and II (Reiner and Rudie 2013), which is a result of using dissolving pulp as a cellulose source material, and because of this the total crystalline area used in this study was considered to be a contribution of both cellulose polymorphs. An example of a deconvoluted XRD pattern can be found in Figure S10 of Supplementary Information.

Transmission electron microscopy (TEM)

The morphology and ultramolecular structure of FDs, NDs, and acetyl grafted CNCs samples were evaluated using TEM. Samples were dispersed in either water or 50/50 % v/v methanol/water. Glow-discharged support grids coated with a formvar + carbon film were floated on sample droplets for 30 s and then floated briefly on droplets of 2 % aqueous Uranyl acetate to negatively stain. Negatively stained images of other types of grafted CNCs could not be obtained due to aggregation in water and methanol and inadequate staining using aqueous electron stains. Samples were imaged using a Philips CM-100 TEM operated at 100 kV, spot 3, 200 µm condenser aperture, and 70 µm objective aperture. Images were captured in digital form using Gatan Orius SC200-1 2Mpixel CCD camera (Gatan, Inc. Pleasanton, CA). The magnification bars were calibrated using replica grating (Ted Pella Inc, Redding, CA-Product# 607). No additional image processing or adjustment was conducted. The dimensions of unmodified and grafted CNCs were measured using the elliptical tool from ImageJ (Hartig 2013). The longest axis of the CNC was defined as length. The maximum dimension of the CNC perpendicular to the length axis was defined as width. 200–300 individual crystals were measured and averaged. Only individual crystals with clearly identifiable edge were measured.

Dispersion study

To evaluate dispersibility, grafted CNCs were dispersed in solvents with different Hansen's solubility parameters (HSP). HSP is a common tool used to evaluate the solubility of polymers in solvent and solvent blends (Hansen 2007). HSPs have three components: dispersion (δ_d), polarity (δ_p), and hydrogen bonding (δ_H). The total solubility parameter (δ_t) can be calculated using Eq. (2), which takes interaction energy represented by all three components into account (Hansen 2007). The solvents used in this study along with their HSP are listed in Table S4 in the Supplementary Information.

$$\delta_t^2 = \delta_d^2 + \delta_p^2 + \delta_H^2 \quad (2)$$

For study of dispersion of grafted samples that were freeze-dried after the reaction, 30 mg of grafted CNCs were sonicated at 20 % amplitude for 2 min in 3 mL of their respective solvents. The final concentration of CNCs was kept at 10 mg/mL. For dispersion study of grafted samples that were kept 'wet' in their prospective washing solvent, the weight percentage of grafted CNCs in the 'wet' samples was first determined gravimetrically. Appropriate amount of 'wet' samples was added to obtain 30 mg of grafted CNCs. Appropriate amount of respective solvent was added so that the final concentration of grafted CNCs was kept at 10 mg/mL. The 'wet' samples were dispersed in their respective solvents using a vortexer. All of the suspensions were left standing overnight to allow possible sedimentation before they were compared.

Dynamic light scattering (DLS)

To evaluate the quality of dispersion, grafted CNC suspensions that had no sedimentations were measured using a Malvern Zetasizer Nano ZS equipped with 633 nm He–Ne laser using a 173 °C scattering angle. The grafted CNC suspensions were diluted with their prospective solvents to 1 mg/mL concentration (0.1 w/v %). The temperature of the suspension was regulated at 25.0 ± 0.1 °C. The apparent hydrodynamic radius was calculated using Stokes–Einstein equation and used as particle size. The suspensions were measured three times. The mean and standard deviation of the measurements were reported.

Results and discussion

Grafting efficiency of esterification methods

Acid anhydride (An), acid catalysis (Ac), acid chloride (Cl), and in situ activator (CDI) mediated esterification reactions of CNC were compared. To understand the role of reaction type on modification and tune the hydrophobicity of CNCs, side chains with different

hydrocarbon lengths were grafted. To provide a fair comparison between different esterification methods, reagents with the same length of hydrocarbon chain were utilized with constant molar ratio between the reagents and the CNC hydroxyl groups for all methods except the acid catalyzed method, which followed the molar ratio suggested by Espino-Pérez et al. (2014). Due to the lack of analogical compounds, transesterification via ring opening polymerization was not included in this study. Both qualitative and quantitative comparisons were conducted on the different esterification methods with respect to the length of hydrocarbon graft.

FT-IR was utilized to qualitatively evaluate the grafting efficiency of each esterification methods used. Figure 2 illustrated the FT-IR spectra of unmodified and grafted CNCs. The spectra were normalized using the C–C stretch at 1060 cm^{-1}. The main demonstration of esterification success was the appearance of carbonyl (C=O) stretch at 1740 cm^{-1}, which was not shown in unmodified CNCs (FD). The changes of other peaks in the fingerprint region after modification could affect the peak height at 1060 cm^{-1} and lead to inaccuracy during normalization and impurities from the different methods complicate results. Nevertheless, the peak height at 1740 cm^{-1} should provide a rough comparison among different esterification methods. Based on the peak height at 1740 cm^{-1}, Fig. 2a indicates that the acid anhydride method provided higher efficiency of grafting for acetyl side chain. The order of grafting efficiency for acetyl grafted CNCs based on FT-IR is: An > CDI ~ Cl > Ac. This might be attributed to the utilization of pyridine as both solvent and catalyst as pyridine was in excess as catalyst and had strong hydrogen bonding reduction property as solvent. For hexanoyl side chain, Fig. 2b demonstrates the grafting efficiency were similar among different methods except for the acid catalyzed method. Figure 2c shows that CDI provided higher efficiency than other reagents for the longest alkyl chain studied. The order of grafting efficiency for dodecanoyl grafted CNCs based on FT-IR is: CDI > Cl > An > Ac. For all three type of structures grafted, the acid catalyzed method did not show significant peak at 1740 cm^{-1}, which indicates that these reactions were unsuccessful or had low efficiency. As stated by Espino-Pérez et al. (2014) the acid catalyzed method required water miscible and high boiling point (>150 °C) carboxylic acids. Hexanoic and dodecanoic acid have limited miscibility with water. Acetic acid has a boiling point relatively close to water. These factors were likely the main reasons that led to unsuccessful grafting using the acid catalyzed method.

To quantitatively analyze the efficiency of each esterification method, ^{13}C solid-state NMR spectroscopy data were collected. The NMR results of unmodified and hexanoyl grafted CNCs, are shown in Fig. 3, while the NMR spectra of the other grafted CNCs can be found in Figure S1–S4 in the Supplementary Information. Signals between 57 and 108 ppm were assigned to the cellulose resonance from CNCs. New signals in the grafted CNC spectra indicate the success of the esterification reaction, in which signals between 15 and 40 ppm were assigned to the grafted aliphatic carbons and signals ranged from 170 to 175 ppm were from the carbonyl carbon. These new signals can be seen most distinctly in the hexanoyl grafted CNC spectra, as shown in Fig. 3. New signals between 18 and 38 ppm (C_8–C_{11}) were assigned to the aliphatic carbons of the hexanoyl moiety in addition to carbonyl (C_7) and terminal (C_{12}) carbon at 172 ppm and 14 ppm, respectively. Similar pattern could be seen in other types of grafted CNCs spectra, suggesting the presence of aliphatic carbons.

Degree of substitution (DS) was calculated to quantitatively compare the different methods. Two methods of calculation from literature were employed to calculate DS. Equation (3) shows the first method, which was introduced by Berlioz et al. (2009)

$$DS_{(C)} = \frac{6 \times I_{CO}}{I_C} \tag{3}$$

I_{CO} is the integral of carbonyl peak. I_C is the integral of all the cellulose carbon peaks. Another method of calculation was first reported by Xiao et al. (2012). Instead of using the carbonyl peak, the terminal carbon peak was used to calculate DS (Eq. 4).

$$DS_{(T)} = \frac{6 \times I_T}{I_C} \tag{4}$$

I_T is the integral of terminal peak. I_C is the integral of all the cellulose carbon peaks. This method of calculation was beneficial in cases where the carbonyl signal was too low due to low collection time.

To check the reproducibility of experiments, hexanoyl grafting reactions were used as a case study. Each experiments were performed twice. The mean

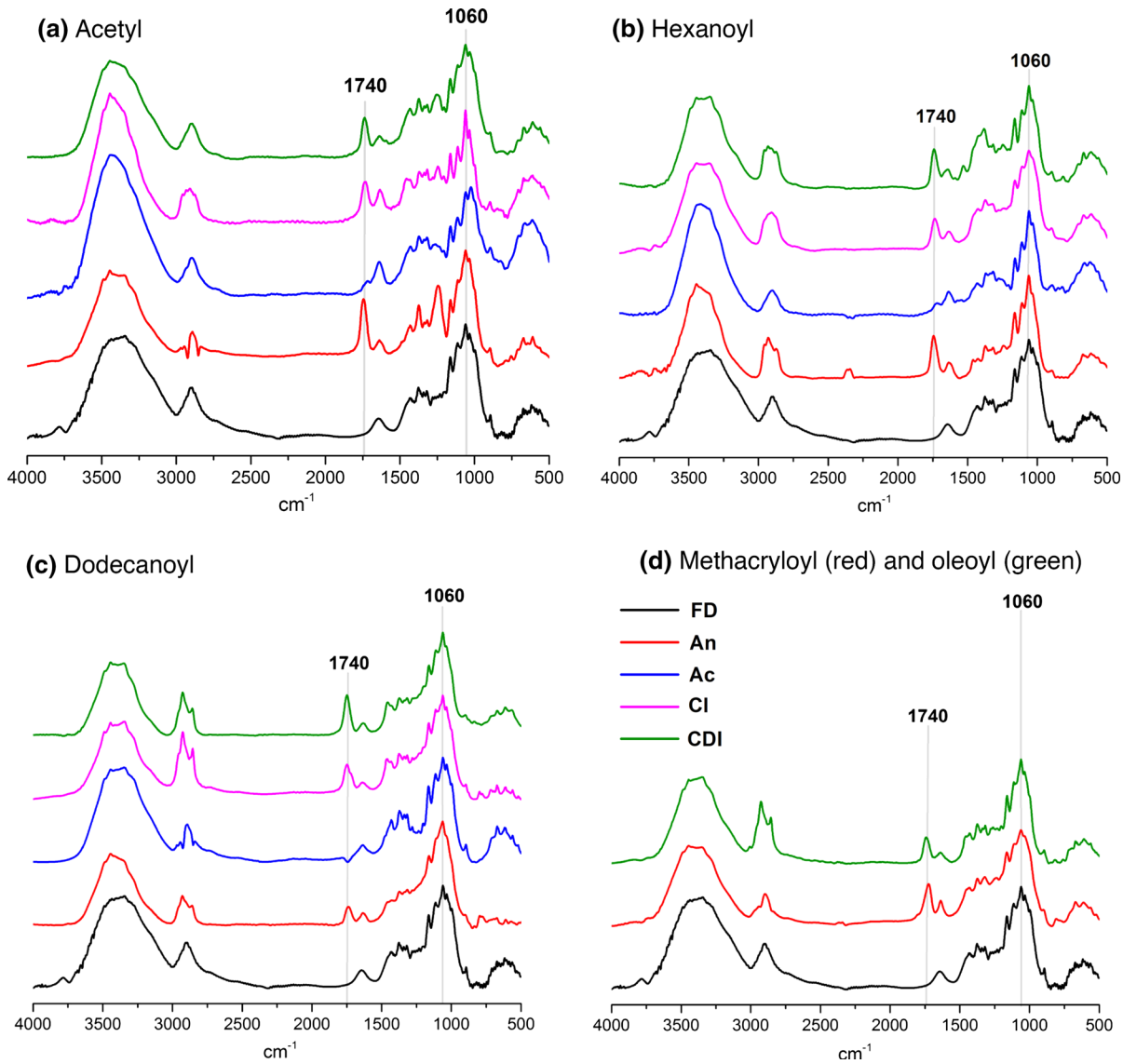

Fig. 2 FT-IR spectra of unmodified and CNCs grafted with **a** acetyl, **b** hexanoyl, **c** dodecanoyl and **d** methacryloyl and oleoyl side chain using acid anhydrides (An), acid catalyzed carboxylic acid (Ac), acid chlorides (Cl), and CDI activated carboxylic acid (CDI). Methacryloyl and oleoyl side groups were only grafted using An and CDI, respectively. Carbonyl peaks at 1740 cm^{-1} indicated grafting success

and standard deviation of the DS values are listed in Table S2. The results indicated that there were no significant differences between the data obtained from the two separate trials. The average DS values for hexanoyl grafted CNCs using different methods were plotted in Fig. 4.

Figure 4 shows that DS is a function of grafted molecule length, and esterification method. For CNCs modified using acid anhydride and acid chloride, DS decreased with increases in grafted molecule length. This was caused by the bulkiness of the reagent leading to lower reactivity. For the CDI activated esterification reaction, high molecular weight carboxylic acids initially had higher grafting efficiency than low molecular weight ones, with DS decreasing as grafting length increases, giving rise to a maximum in DS at the hexanoyl grafted samples. When comparing between the esterification methods, acid

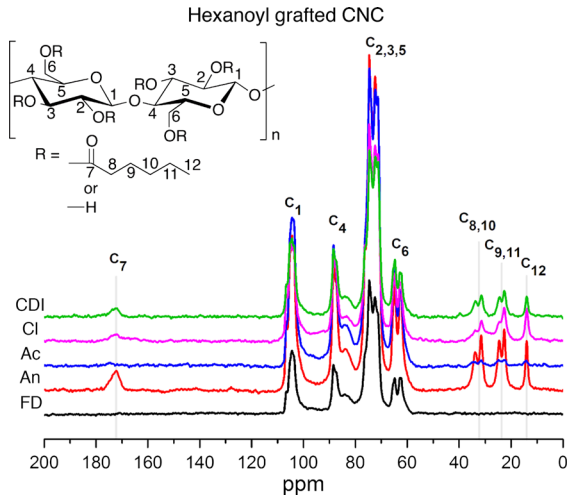

Fig. 3 ^{13}C solid-state NMR spectra of unmodified (FD) and hexanoyl grafted CNCs using different methods (An, Ac, Cl, and CDI)

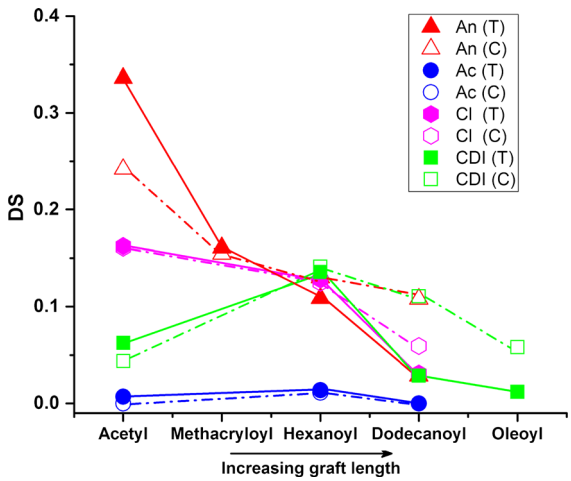

Fig. 4 Degree of substitution (DS) of different esterification methods (An, Ac, Cl, and CDI) with respect to the grafted moieties calculated using carbonyl (C) and terminal (T) carbon integration method with Eqs. (3) and (4), respectively

anhydride had the highest grafting efficiency than other reagents for low molecular weight moieties. The difference in grafting efficiency between the different esterification methods is most apparent in acetyl grafted CNCs. For hexanoyl grafted CNCs, the efficiency was similar among all the methods except the acid catalyzed method agreeing with the FT-IR data. According to the calculation method using the carbonyl carbon, CDI and acid anhydride had higher efficiency than acid chloride for dodecanoyl grafted samples, while the terminal carbon calculation showed that all three methods were similar.

In addition to solid-state NMR study, elemental analysis was utilized to verify the trend found. All grafted CNCs using FD starting materials were measured for their Carbon, Hydrogen, and Oxygen content. The results were listed in Table S3 of the Supplementary Information. The experimental results were corrected to take account of the impurities and surface sulfate half-ester of the starting material (Siqueira et al. 2010). The absolute DS values calculated with elemental analysis is higher than the values calculated with NMR. However, the DS trends found using these two techniques were similar. The higher DS value is likely due to the presence of impurity in the modified material that did have the expected chemical shift in solid state NMR. Therefore, they were not included in the NMR DS calculation. For acetyl and hexanoyl grafted CNCs using CDI, the presence of unexpected nitrogen content also indicated possible impurities from CDI activated carboxylic acids, which were difficult to remove due to their similar solubility as grafted CNCs. However, as longer side groups were grafted, nitrogen content impurities were not present.

To further demonstrate the versatility of the esterification reactions, functional moieties that contain terminal or internal double bonds such as methacryloyl and oleoyl were also grafted. These active moieties can potentially polymerize or crosslink during the esterification reaction, which can lead to undesirable side reactions and the loss of functionality. Therefore, an appropriate esterification reagent needs to be selected. In this study, acid anhydride was chosen to graft methacryloyl side group due to the higher DS that the method affords, while CDI was used to graft the oleoyl side group since oleic acid is relative inexpensive versus its anhydride counterpart. The characterization results for methacryloyl and oleoyl grafted CNCs are also illustrated in Figs. 2 and 4. Similar to other esterification reactions, the grafting of these moieties was successful. As shown in Figures S3 and S4, the double bonds structures of the grafted moieties were also preserved after both reactions. Side reactions of the unsaturated side groups were suppressed, as no extensive crosslinking of the product was observed. These results indicate that acid anhydride and CDI can tolerate internal and terminal double bond, respectively. In terms of grafting

efficiency of these unsaturated moieties, methacryloyl grafted CNCs using acid anhydride followed the trend suggested by other acid anhydride modified moieties. As shown in Fig. 4, oleoyl grafted CNC using CDI followed a similar grafting efficiency order suggested by the trend as the low reactivity of the relatively long aliphatic carbon chain of oleic acid continues reduction in DS.

Morphology and dimensions of grafted CNCs

The trend found in Fig. 4 provided a preliminary guide to select the most efficient reagent to graft CNCs with aliphatic carbons. Nevertheless, to be a viable grafting method, the esterification reaction needs to preserve the morphology and crystallinity of CNC. TEM microscopy was utilized to evaluate the effect of different esterification methods on the morphology and dimensions of the CNCs. TEM micrographs of unmodified and acetyl grafted CNCs (see Figure S5 in the Supplementary Information) were used to estimate particle dimensions, results are summarized in Fig. 5. The histograms of the measurements are given in Supplementary Information Figures S6–S8. When the CNC source materials were compared with each other, the never-dried CNCs (ND) had higher aspect ratio than freeze-dried CNCs (FD). The difference between ND and FD could be due to batch to batch variation of the CNC production process, agglomeration of FD CNC that could not be broken up when redispersed in water, TEM sample to sample variation, etc. Student's t-tests were conducted between the measurements of unmodified starting material (FD or ND) and grafted materials. The only statistically relevant decrease is that acid catalyzed samples had lower aspect ratio than the never-dried CNC starting material. All other acetyl grafted samples had statistically higher crystal dimensions than their starting material. This is likely attributed to low image contrast and large amounts of aggregation that was observed in acid catalyzed and acid chloride modified samples, which led to measurement inaccuracies. This observation agreed with previous report that protonated acid-form of CNC aggregates in water once dried (Dong and Gray 1997). Also, surface modified CNCs could potentially have different affinity toward TEM staining agent than unmodified CNCs. Notwithstanding these effects, no major changes were observed in crystal size or morphology.

Crystallinity of grafted CNCs

To investigate the effect of esterification on crystallinity of the CNCs, X-ray diffractograms of unmodified and grafted CNCs were collected and illustrated in Fig. 6. Cellulose Iβ is the dominant polymorph from higher-plant cells (Belton et al. 1989) and the diffraction profile contains peaks that represent (110), $(1\bar{1}0)$, (012), (200), and (004) lattice planes (Sugiyama et al. 1991). These peaks can be located in Fig. 6 at 2θ angles of 15.6°, 17.5°, 21°, 23°, and 35.3°, respectively. The unusual high intensity of the peak at 21° represents the existence of cellulose II [i.e. the (110) lattice plane from cellulose II] (Kim et al. 2013), which is typical of CNCs from FPL, an artifact of using dissolving pulp as the source material (Reiner and Rudie 2013). In general, there were no drastic changes in the diffraction pattern after the esterification reactions. No additional peaks appeared after the esterification process, which demonstrated that there were no cellulose II converted after the process. To check whether the esterification method converted crystalline cellulose to amorphous cellulose, the crystallinity of unmodified and grafted CNCs were calculated and compared. As shown in Table 1, for some of the esterification methods, there was up to 8.5 % decrease in crystallinity after grafting. However, inaccuracy might have been introduced due to the appearance of new peaks corresponding to aliphatic chains around 21° after grafting (Habibi and Dufresne 2008; Junior de Menezes et al. 2009). Therefore, more evidence was needed to evaluate the crystallinity of the grafted CNCs.

To further analyze the crystallinity of unmodified and grafted CNCs, the ^{13}C NMR C4 carbon peak separation methods developed by Newman (2004) were used to calculate crystallinity index (CI). The C4 carbon region of unmodified CNC was illustrated in Fig. 7. The integral area from 85.5 to 91 ppm was assigned to the ordered cellulose, while integral area between 80.3 and 85.5 ppm was assigned to disordered cellulose (Ibbett et al. 2007; Sèbe et al. 2012; Kim et al. 2013; Gårdebjer et al. 2015). CI was calculated by dividing the crystalline region over the entire C4 carbon region (integral area between 80.3 and 91 ppm). The CI of both unmodified CNC and grafted CNC are also listed in Table 1. The data indicates that after grafting there was minimal

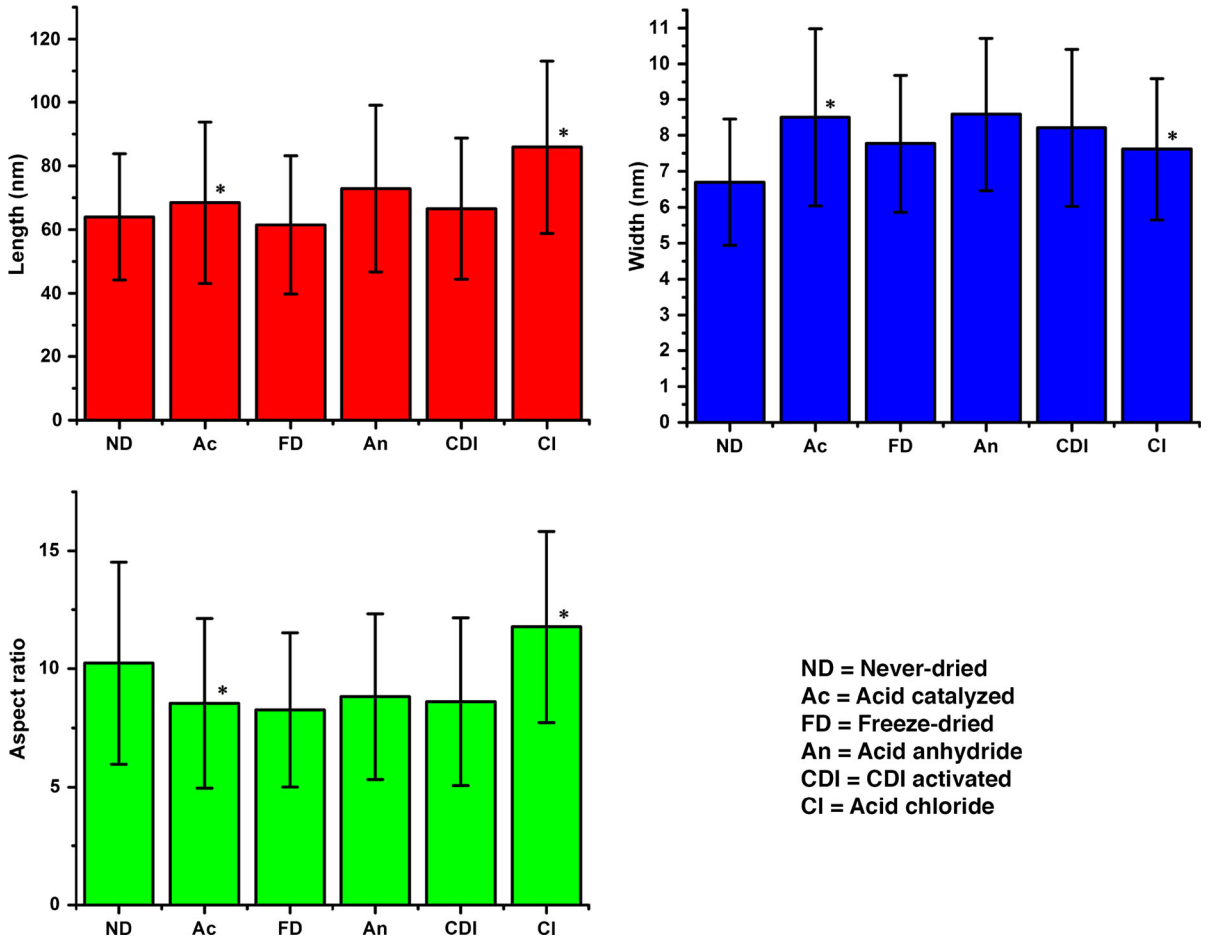

Fig. 5 Summary of average dimensions of unmodified (ND and FD) and acetyl grafted CNCs using Ac, An, Cl, and CDI esterification methods. *Asterisk* inaccuracy might be introduced due to aggregation of crystals that lead to measurement difficulties. *Error bars* indicate standard deviation

decrease in crystallinity and in some cases the crystallinity appears to increase. The increase in crystallinity could be due to the inaccurate peak integration caused by low NMR signal intensity. The similar increases were also observed in the XRD data, while changes in crystallinity may be occurring, such changes are modest in comparison to the variability in data. Hence, few trends could be observed. To investigate the change in crystallinity and degree of substitution, changes of crystallinity measured using XRD and NMR methods were plotted against degree of substitution calculated from solid state NMR. The results were plotted in Figure S9. There is no clear trend that can be observed that indicated changes in crystallinity increased with higher degree of substitution.

Overall, to choose the most viable esterification method to modify CNCs, multiple factors have to be considered. Depending on the final application, the structure of grafted moiety or side group is predetermined, which dictates the types of reagents and esterification method that were allowed. The commercial availability of reagent structures, especially acid anhydrides and acid chlorides, limits the use of certain esterification methods. Similarly, acid catalyzed esterification reactions require water miscible and high boiling point carboxylic acids. In situ activator such CDI can resolve this issue, since it enables the use of a broad variety of complex carboxylic acids (Hussain et al. 2004; Heinze et al. 2006). However, CDI has limitation when dealing with moieties with active protons such as terminal

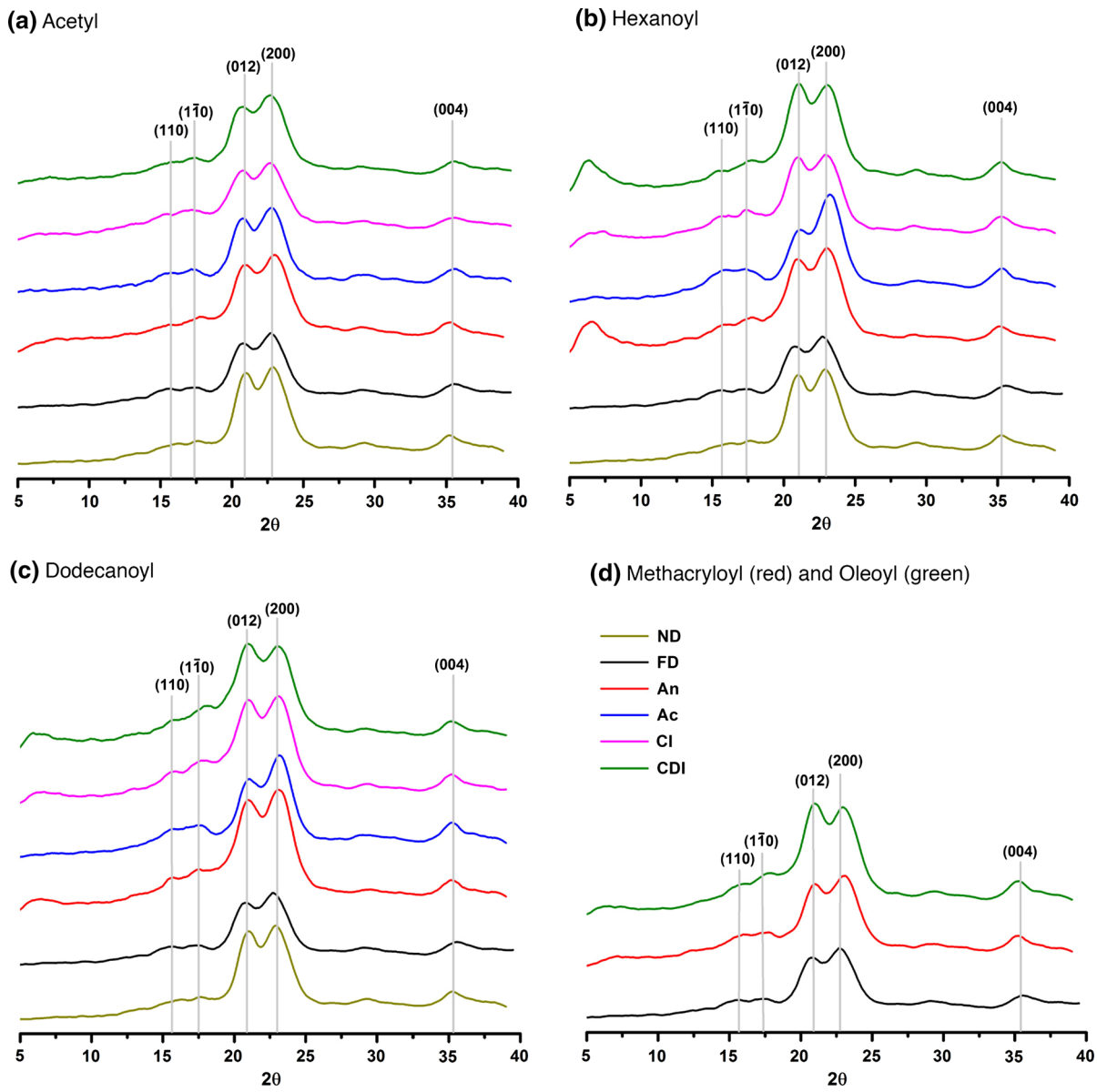

Fig. 6 X-ray diffractograms of never-dried CNC (ND), freeze-dried CNC (FD), and acetyl (**a**), hexanoyl (**b**), dodecanoyl (**c**), and methacryloyl and oleoyl (**d**) grafted CNCs using various esterification methods (An, Ac, Cl, and CDI)

double or triple bonds (Heinze et al. 2006). Price of the reagents is also important to consider. Acid anhydride and acid chloride are generally more expensive than their carboxylic acid counterparts. In recent years, decrease in price of production of CDI has enabled it to become an affordable option (Heinze et al. 2006). The ease and simplicity of the reaction process is also a critical factor. For reaction time, CDI mediated reaction requires an extra carboxylic acid activation step that lasts longer than other esterification reactions. In terms of reaction condition, almost all esterification reagents were sensitive to water, hence prohibit the use of water as reaction solvent. The acid catalyzed method developed by Espino-Pérez et al. (2014) has an advantage over other methods as it eliminates the use of solvent. Other solvent-less reactions can also be found in literature (Herrick et al. 1983; Berlioz et al. 2009). However, the versatility of these methods is

Table 1 Crystallinity calculated using the XRD peak deconvolution method and the NMR peak separation method

Grafted moieties	Grafting method	% Crystallinity (from XRD)	% Change after grafting (from XRD)	% Crystallinity (from SSNMR)	% Change after grafting (from SSNMR)
ND		75.5		66.7	
FD		73.0		63.0	
Acetyl	Ac	77.6	6.3	65.6	4.0
	An	73.4	0.5	62.7	−0.5
	Cl	74.5	2.1	65.2	3.4
	CDI	71.7	−1.8	68.1	8.0
Hexanoyl	Ac	81.2	9.9	64.7	2.6
	An	70.0	−4.1	65.9	4.6
	Cl	70.6	−3.3	70.5	11.8
	CDI	78.7	7.8	67.7	7.4
Dodecanoyl	Ac	78.8	7.9	62.9	−0.3
	An	75.1	2.9	70.9	12.5
	Cl	70.0	−4.1	70.5	11.8
	CDI	69.4	−4.9	71.7	13.7
Methacryloyl	An	73.5	0.7	65.3	3.5
Oleoyl	CDI	77.9	6.7	72.0	14.3

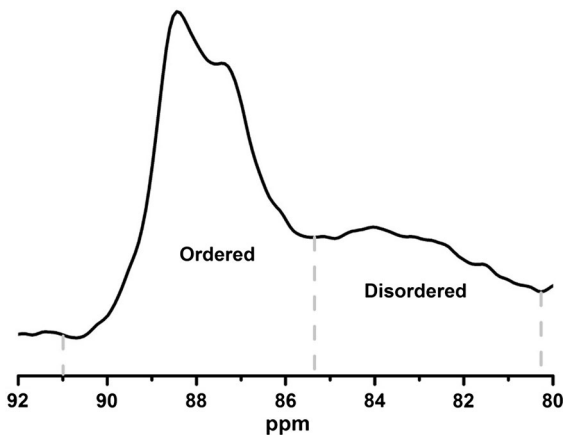

Fig. 7 Evaluation of CNC crystallinity via ^{13}C solid state NMR spectroscopy at the C4 carbon

unknown. The ease of purification is another important factor. Acid chloride reaction produces HCl as side product, which is either evolved during the reaction or trapped by TEA or pyridine. The TEA or pyridine HCl complex has to be removed by washing. Acid anhydride reactions provide an equivalent mole of carboxylic acid as side product, which is difficult to remove due to their similar solubility as grafted CNCs. For acid catalyzed reaction, the side product is water, which is continually removed during the reaction. CDI mediated reactions produce imidazole and CO_2 as side product. Imidazole is freely soluble in different solvents and can be easily removed (Heinze et al. 2006). Ultimately, the final application drives the esterification process. Regardless, on balance for short chain or widely available reagents, anhydride grafting is optimal. For surface modifications where the acid anhydride is relatively expensive, CDI grafting is the better choice.

Dispersibility of grafted CNCs in organic solvents

A primary goal of hydrophobization of CNCs is to improve their compatibility and dispersibility in hydrophobic media. Figure 8 illustrates freeze-dried unmodified and grafted CNCs dispersed in solvents (water, ethanol, acetone, THF, and toluene). For acetyl and methacryloyl groups, acid anhydride method was used for grafting reaction. For hexanoyl, dodecanoyl, and oleoyl groups, CDI method was used. For each type of grafted CNCs, the final products were freeze-dried and then added to the solvents. The suspensions were sonicated and left overnight to let the residual energy from sonication to dissipate and allow for observation of sedimentation height. As shown in Fig. 8, the dispersibility of grafted CNC depends both on DS and the length of the aliphatic chain grafted.

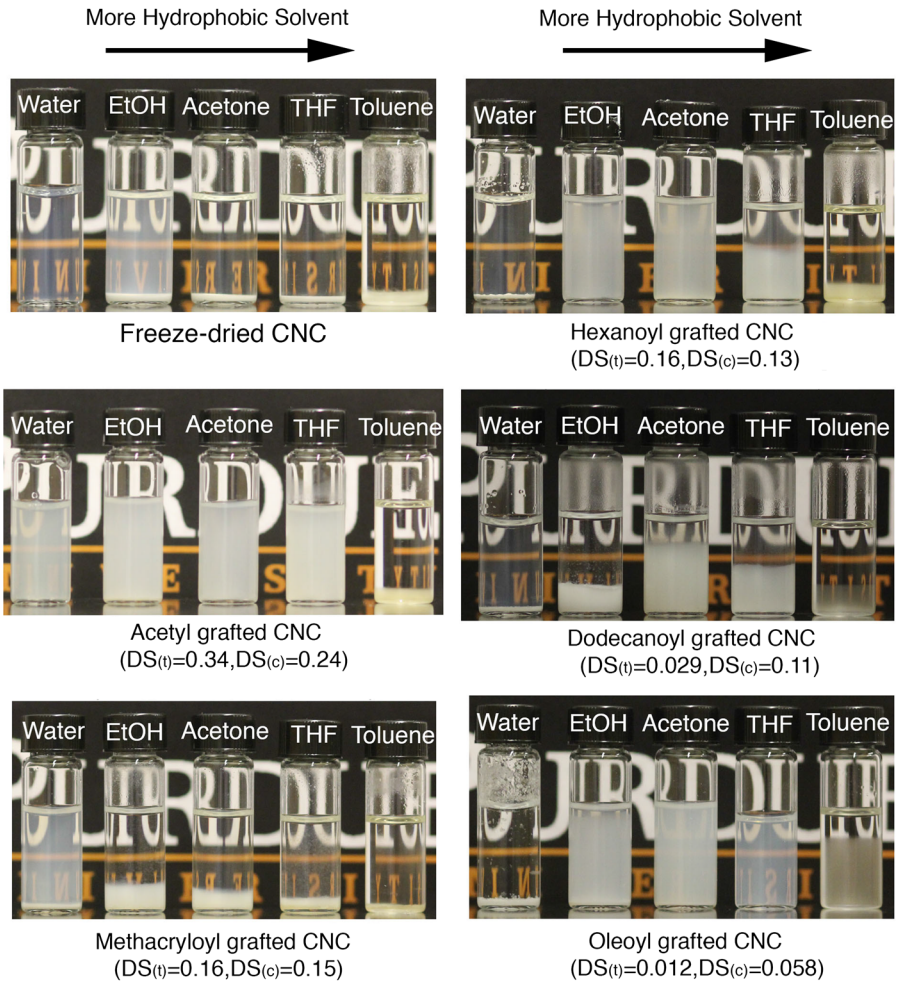

Fig. 8 Dispersion of unmodified freeze-dried CNCs and grafted CNCs in solvents. Freeze-dried CNCs are used as starting materials for the grafting reactions. The grafted CNCs were freeze-dried before redispersion. The concentration of CNCs was kept at 10 mg/mL

Acetyl grafted CNCs had better dispersibility in different organic solvent than methacryloyl grafted CNCs despite having fewer hydrocarbons in their side chain. Even compared to hexanoyl grafted CNCs, acetyl grafted did not sediment in THF while hexanoyl grafted CNC did. This effect was due to acetyl grafted CNCs having higher DS than methacryloyl and hexanoyl grafted CNCs. Similar phenomenon could be seen between hexanoyl and dodecanoyl grafted CNCs. However, as length of the aliphatic chain became longer, the dispersibility improved even at low DS value. Oleoyl grafted CNCs could form stable dispersion in THF regardless having the lowest DS value. The better transparency of the oleoyl grafted CNC suspension in THF indicated that particle aggregation size was smaller, which demonstrated better dispersion. Overall, the dispersibility of grafted CNCs after freeze-drying was low, which could be attributed to the hydrogen bonding of residual unreacted hydroxyl groups on the CNC surface.

To improve dispersibility, grafted CNCs were kept in their washing solvent after centrifugation as concentrated gel-like form. These 'wet' samples were then redispersed in organic solvents (water, ethanol, acetone, THF, and toluene. For oleoyl grafted CNC, cyclohexane and hexane were also included to extend the solvency range of grafted CNC). For comparison, never-dried CNCs were also dispersed in these solvents. Figure 9 shows the images of these suspensions from 'wet' samples. The presence of residual washing solvent altered the HSP value of the final solvent in the suspension. The HSP of the solvent mixture used in Fig. 9 were calculated using the individual HSP components of each solvent and their

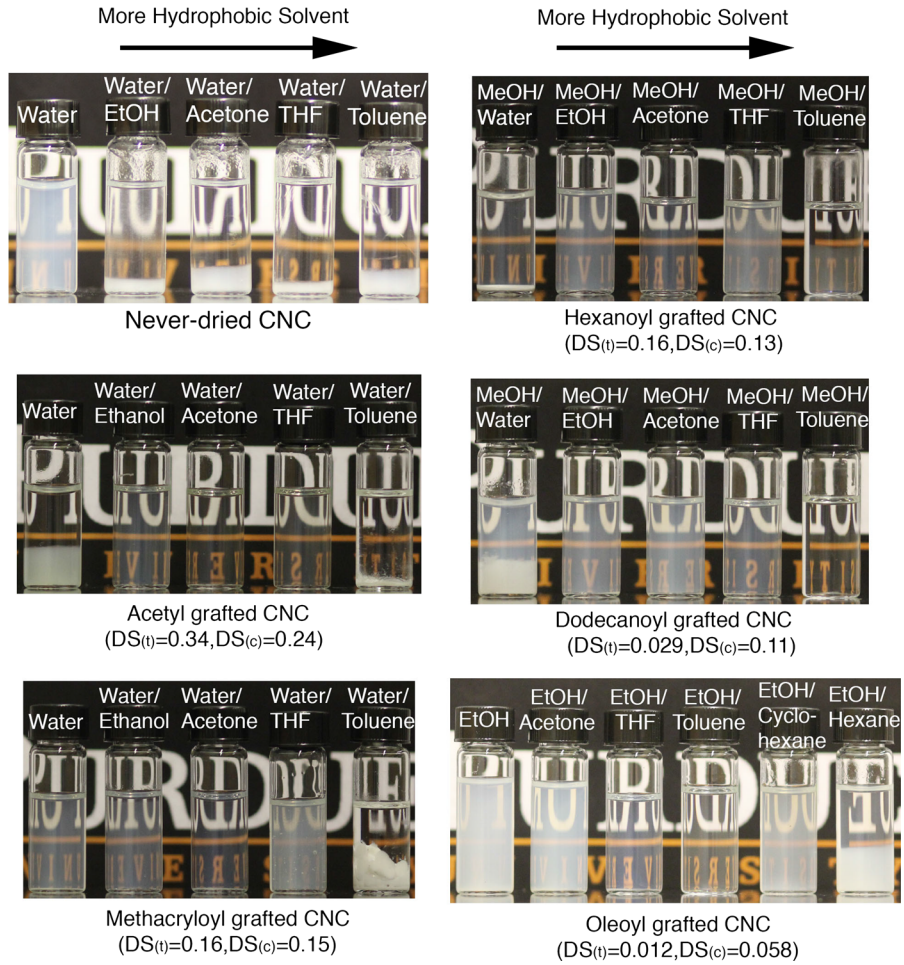

Fig. 9 Dispersion of unmodified never-dried CNC and 'wet' grafted CNCs in solvents. Residual washing solvent from the 'wet' grafted CNC and the test solvent created solvent mixtures. Freeze-dried CNCs are used as starting materials for the grafting reactions. The final concentration of CNCs was kept at 10 mg/mL

volume ratio (Hansen 2007). The detailed results were listed in Table S5 in the Supplementary Information. Due to the low content of the washing solvent, the overall HSP value of the solvent mixture did not change drastically when compared to that of the pure solvent. However, as shown in Fig. 9, the dispersibility of grafted CNCs was improved overall when they were kept as 'wet'.

Teas plots were created and illustrated in Fig. 10 for each types of grafted CNC using fractional HSP for solvent and solvent mixture used in the dispersibility test. Completely dispersed samples were marked as solid colored dots. Semi-dispersed sample with sedimentation height higher than half of its original height were marked as light colored dots. Samples with sedimentation height lower than half of its original height were marked as hollow dots. Base on available data, dispersibility windows of grafted CNCs were estimated by outlining around the solid colored dots and overlapping the light colored dots. As shown in Fig. 10, the dispersibility windows for 'wet' grafted CNCs generally increased in size and shifted toward the lower right corner as compared to the freeze-dried grafted CNCs. When freeze-dried grafted CNCs were sonicated in the same solvent mixture as their 'wet' counterparts, they could not be dispersed. This effect further indicated that the low dispersibility was due to the dried CNCs forming strong hydrogen bonds that lead to aggregation. The Teas plot can also serve as a comparison tool for dispersing grafted CNC into

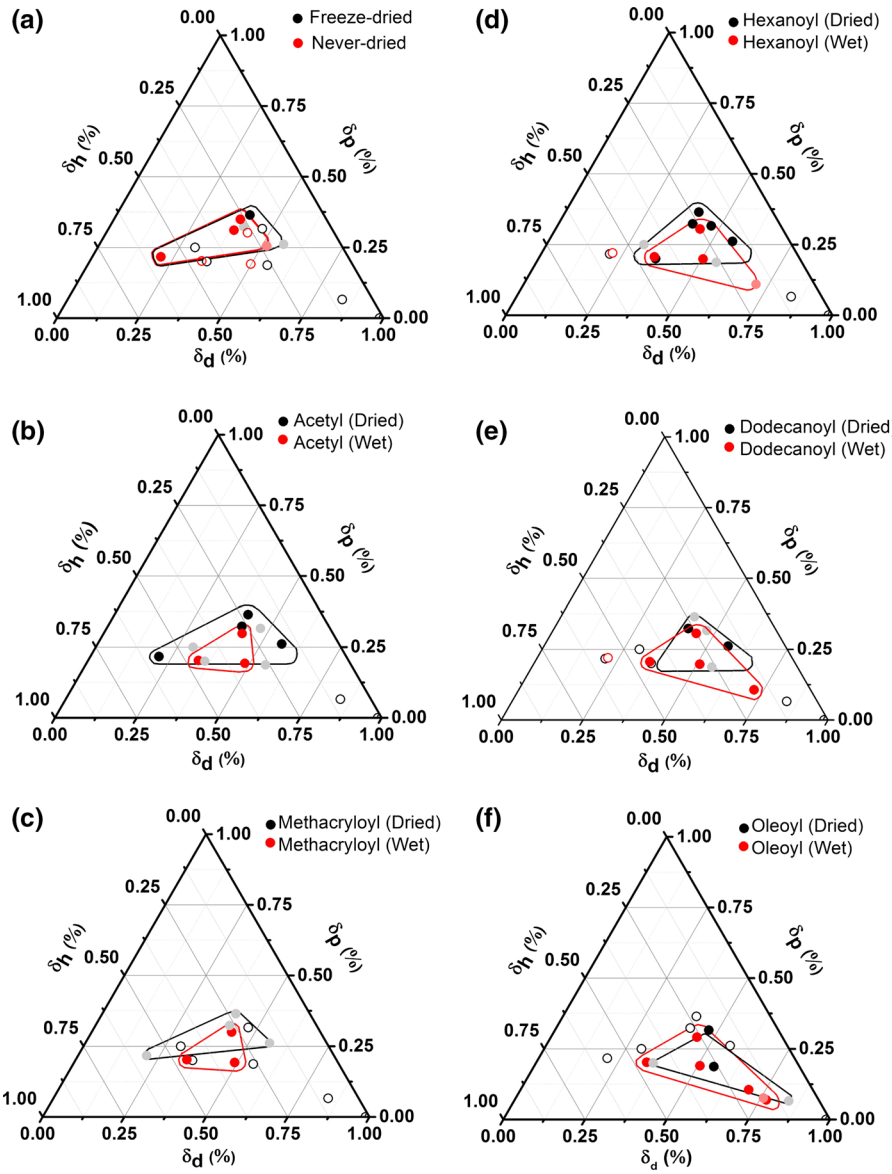

Fig. 10 Teas plots of unmodified (Part **a**) and grafted CNCs (Part **b**–**f**). The grafted CNCs were kept in freeze-dried and 'wet' form. Residual wash solvents from the 'wet' form were taken into account

polymer. A certain polymer that has a solubility window in similar region on the Teas plot as a type of grafted CNC should have good compatibility.

As suggested by Tian et al. (2014) grafted CNCs using freeze-dried and solvent-exchanged starting materials have different dispersibility and surface accessibility. To evaluate this effect, additional trials of esterification reactions were conducted utilizing never-dried CNCs that were solvent-exchanged from water. The CDI esterification method was chosen as it was easily amenable toward the use of never-dried CNCs. Dodecanoyl and oleoyl groups were grafted. These grafted CNCs were also kept in both freeze-dried and 'wet' form. Figure 11 illustrated the images for these suspensions. The dispersibility of dodecanoyl and oleoyl grafted CNC were improved when solvent exchanged source materials were used. For oleoyl grafted CNCs, the dispersibility in ethanol and acetone was decreased. This effect indicated that overall hydrophobicity of oleoyl grafted was improved. These result agreed with the trend found by Tian et al. (2014). A similar trend could be seen

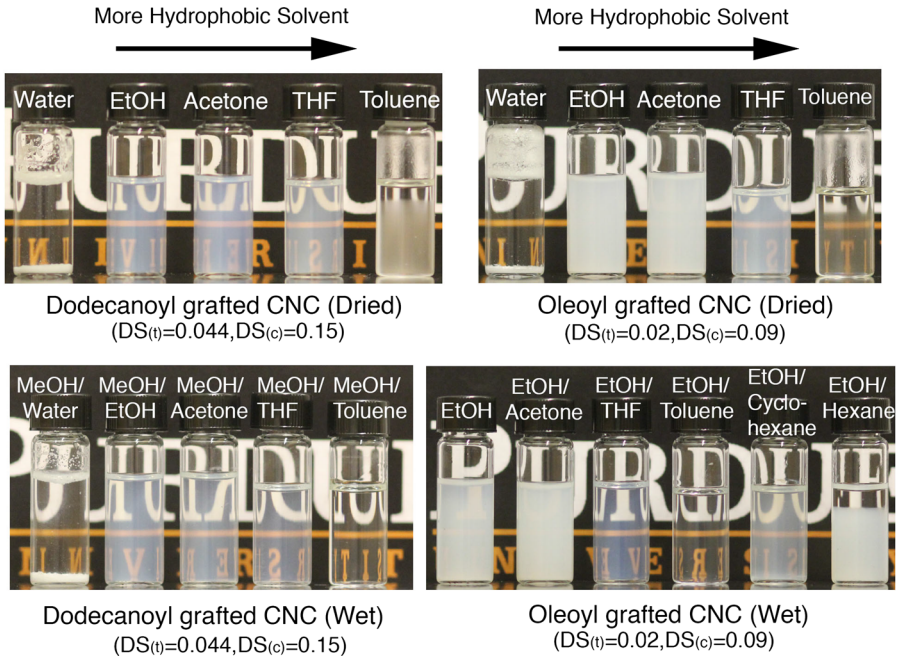

Fig. 11 Dispersion of grafted CNCs in solvents using never-dried CNCs as starting materials. Samples in the *top* two images were freeze-dried after the reaction. Samples in the *bottom* two images were kept 'wet' in their washing solvents. The final concentration was kept at 10 mg/mL

when these grafted CNCs were kept 'wet', as shown in bottom images of Fig. 11. When comparing between 'wet' oleoyl grafted CNCs in Figs. 9 and 11, samples from solvent exchanged source materials had lower sedimentation in hexane than samples using freeze-dried source materials. The higher dispersibility of grafted CNCs using solvent exchange materials was likely due to the surface hydroxyl group being more accessible for modification. As shown in Fig. 8 and 11, the DS values for grafted CNC using solvent exchanged starting material was higher than their freeze-dried counterparts.

To further evaluate the dispersion of grafted CNC in solvents, DLS was utilized to determine the size of grafted CNC aggregation. The apparent hydrodynamic radius of the suspensions was calculated and illustrated in Fig. 12. FD and ND suspensions in water were used as reference as shown in Fig. 12a. The hydrodynamic radius measured for FD and ND CNCs agreed with the TEM results in Fig. 5. ND CNC suspension that was not sonicated had small aggregation close to 120 nm. For dodecanoyl grafted CNCs in Fig. 9, samples with no sedimentation were measured and compared in Fig. 12b. The DLS results indicated the aggregation size increased as solvent became more hydrophobic. This is likely attributed by the low DS value. For other grafted CNC dispersions, acetone was used as the solvent of interest. As shown Fig. 12c, for grafted CNCs that used FD as starting materials, dried samples had either had sedimentation (methacryloyl and dodecanoyl) or larger aggregations than 'wet' samples. These results further suggested that keeping the samples 'wet' is a viable method to obtain good dispersion in solvent. For dodecanoyl and oleoyl grafted samples using ND starting material in Fig. 12d, dried and 'wet' samples had similar aggregation size in acetone. Compare to Fig. 12c, these samples had smaller aggregation than their freeze-dried counterparts in general. This is likely due to the higher DS of the samples using ND starting material.

The potential mechanism behind the improved dispersibility of 'wet' grafted CNCs was that the washing solvents served as a compatibilizer for the bulk solvent. The washing solvent used in this study was water, methanol, or ethanol. These solvents, especially ethanol, are miscible with various hydrophobic solvents. In addition, they have hydroxyl groups that can form hydrogen bonds, which can potentially bound with unreacted residual surface hydroxyl groups on the CNCs and block their interactions with each other and

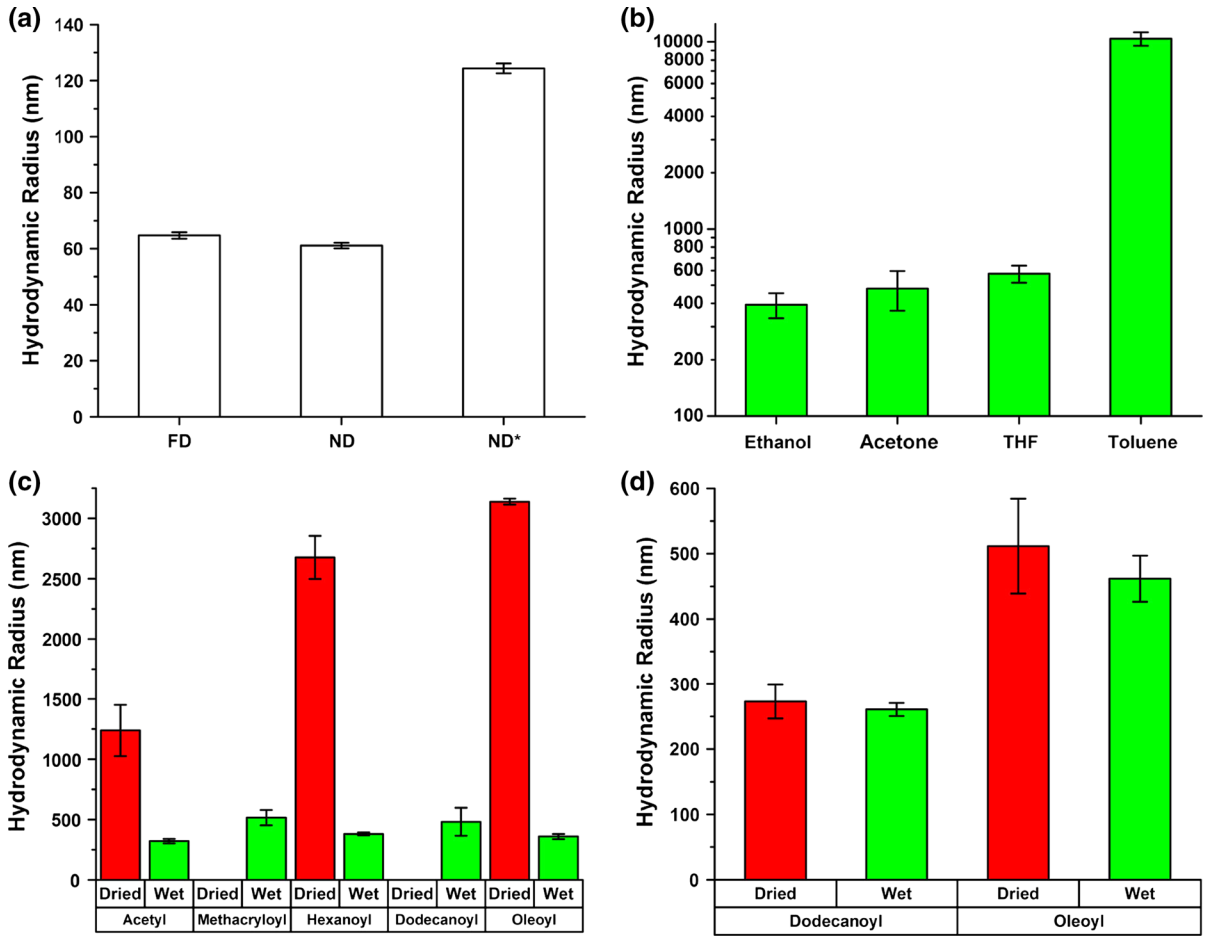

Fig. 12 Dimensions of unmodified and grafted CNCs in solvents determined by DLS. **a** Sonicated FD and ND CNC suspensions in water. *ND** ND suspension that was not sonicated. **b** Wet dodecanoyl grafted CNC from Fig. 9 in various solvents. **c** Various types of grafted CNC from Figs. 8 and 9 in acetone. **d** Dodecanoyl and oleoyl grafted CNCs using ND starting material from Fig. 11 in acetone

the organic solvent. Hence, the dispersibility of grafted CNCs was improved by preventing aggregation. The potential mechanism of action was illustrated in Fig. 13. By utilizing this method, the range of dispersibility of grafted CNCs was expanded. As shown in Fig. 11, dodecanoyl grafted CNCs were able to disperse in ethanol, acetone, THF, and toluene with less than 10 % by volume of methanol. Potentially, other more hydrophobic solvent could be used as washing solvent to further improve the dispersibility of the grafted CNCs in hydrophobic media. However, the product yield of the extraction process using different washing solvents requires further investigation. For nanocomposite applications, CNCs, as fillers, can form hydrogen bonds between each other and lead to a percolation network that improves the mechanical properties of the overall nanocomposite (Capadona et al. 2008). However, surface modification with high DS could decrease the ability of CNCs to form percolation networks despite improving their dispersibility in the polymer matrix. In order to manage these two competing effects, a balance needs to be found during surface modification. The mechanism proposed in this study could improve the dispersibility of modified CNCs while preserving their capability to form hydrogen-bonding networks. However, there is need for precise control of degree of substitution in order to explore the relationship between surface modification and hydrogen bonding capability of CNCs.

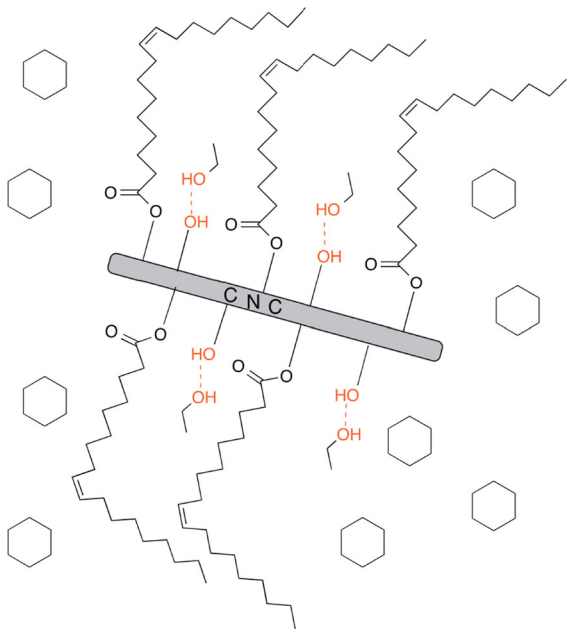

Fig. 13 Proposed mechanism of ethanol acting as compatibilizer for oleoyl grafted CNCs in cyclohexane

Conclusion

Surface esterification methods of CNCs via acid anhydride, acid chloride, acid catalyzed carboxylic acid, and in situ activated carboxylic acid were compared. Acid anhydride had better grafting efficiency than other reagents for low molecular weight moieties with short aliphatic chains. For long chain aliphatic grafts, utilizing CDI was more viable approach due to more availability of grafting moieties in carboxylic acid form. The ultramolecular structure and crystallinity were not affected by the grafting reactions. The dispersibility of grafted CNCs in organic solvents could be improved by utilizing never-dried CNCs before the reactions and kept the grafted CNCs wet after the reaction. The washing solvents served as a compatibilizer for these wet grafted CNCs and expanded the range of their hydrophobic dispersibility.

Supplementary information

Accessible surface hydroxyl group calculation of FD and ND CNC, Table of reagents and detailed experimental condition, ^{13}C solid-state NMR spectra of acetyl, dodecanoyl, methacryloyl, and oleoyl grafted CNC, Table of degree of substitution of hexanoyl grafted CNC using different method calculated with solid state NMR, Table of elemental analysis results and degree of substitution of hexanoyl grafted CNC using different method, TEM images of acetyl grafted CNCs, histograms of TEM dimension measurement of acetyl grafted CNCs, Graphs of Degree of substitution versus % crystallinity changes for different types of grafting, and tables of Hanson's solubility parameters of solvent and solvent mixture used in this study.

Acknowledgments The authors would like to thank John Harwood from Purdue Interdepartmental NMR Facility for obtaining the ^{13}C solid-state NMR spectra. The research was supported by the National Science Foundation IGERT sustainable electronic Grant #1144843-DGE and the Forest Products Laboratory under USDA Grant: 11-JV-11111129-118.

References

Araki J, Mishima S (2014) Steric stabilization of "charge-free" cellulose nanowhiskers by grafting of poly(ethylene glycol). Molecules 20:169–184. doi:10.3390/molecules20010169

Araki J, Wada M, Kuga S, Okano T (1998) Flow properties of microcrystalline cellulose suspension prepared by acid treatment of native cellulose. Colloids Surf A Physicochem Eng Asp 142:75–82. doi:10.1016/S0927-7757(98)00404-X

Beck-Candanedo S, Roman M, Gray DG (2005) Effect of reaction conditions on the properties and behavior of wood cellulose nanocrystal suspensions. Biomacromolecules 6:1048–1054. doi:10.1021/bm049300p

Belton PS, Tanner SF, Cartier N, Chanzy H (1989) High-resolution solid-state carbon-13 nuclear magnetic resonance spectroscopy of tunicin, an animal cellulose. Macromolecules 22:1615–1617. doi:10.1021/ma00194a019

Bendahou A, Hajlane A, Dufresne A et al (2014) Esterification and amidation for grafting long aliphatic chains on to cellulose nanocrystals: a comparative study. Res Chem Intermed. doi:10.1007/s11164-014-1530-z

Berlioz S, Molina-Boisseau S, Nishiyama Y, Heux L (2009) Gas-phase surface esterification of cellulose microfibrils and whiskers. Biomacromolecules 10:2144–2151. doi:10.1021/bm900319k

Boujemaoui A, Mongkhontreerat S, Malmström E, Carlmark A (2015) Preparation and characterization of functionalized cellulose nanocrystals. Carbohydr Polym 115:457–464. doi:10.1016/j.carbpol.2014.08.110

Braun B, Dorgan JR (2009) Single-step method for the isolation and surface functionalization of cellulosic nanowhiskers. Biomacromolecules 10:334–341. doi:10.1021/bm8011117

Braun B, Dorgan JR, Hollingsworth LO (2012) Supra-molecular ecobionanocomposites based on polylactide and cellulosic

nanowhiskers: synthesis and properties. Biomacromolecules 13:2013–2019. doi:10.1021/bm300149w
Cao Y, Zavaterri P, Youngblood J et al (2015) The influence of cellulose nanocrystal additions on the performance of cement paste. Cem Concr Compos 56:73–83. doi:10.1016/j.cemconcomp.2014.11.008
Capadona JR, Van Den Berg O, Capadona LA et al (2007) A versatile approach for the processing of polymer nanocomposites with self-assembled nanofibre templates. Nat Nanotechnol 2:765–769. doi:10.1038/nnano.2007.379
Capadona JR, Shanmuganathan K, Tyler DJ et al (2008) Stimuli-responsive polymer nanocomposites inspired by the sea cucumber dermis. Science 319:1370–1374. doi:10.1126/science.1153307
Cetin NS, Tingaut P, Ozmen N et al (2009) Acetylation of cellulose nanowhiskers with vinyl acetate under moderate conditions. Macromol Biosci 9:997–1003. doi:10.1002/mabi.200900073
Chen S, Schueneman G, Pipes RB et al (2014) Effects of crystal orientation on cellulose nanocrystals–cellulose acetate nanocomposite fibers prepared by dry spinning. Biomacromolecules 15:3827–3835. doi:10.1021/bm501161v
Diaz JA, Wu X, Martini A et al (2013) Thermal expansion of self-organized and shear-oriented cellulose nanocrystal films. Biomacromolecules 14:2900–2908. doi:10.1021/bm400794e
Diaz JA, Ye Z, Wu X et al (2014) Thermal conductivity in nanostructured films: from single cellulose nanocrystals to bulk films. Biomacromolecules 15:4096–4101. doi:10.1021/bm501131a
Dixon W, Schaefer J, Sefcik M et al (1982) Total suppression of sidebands in CPMAS C-13 NMR. J Magn Reson 49:341–345. doi:10.1016/0022-2364(82)90199-8
Dong XM, Gray DG (1997) Effect of counterions on ordered phase formation in suspensions of charged rodlike cellulose crystallites. Langmuir 13:2404–2409. doi:10.1021/la960724h
Dong S, Roman M (2007) Fluorescently labeled cellulose nanocrystals for bioimaging applications. J Am Chem Soc 129:13810–13811. doi:10.1021/ja076196l
Elazzouzi-Hafraoui S, Nishiyama Y, Putaux J-L et al (2008) The shape and size distribution of crystalline nanoparticles prepared by acid hydrolysis of native cellulose. Biomacromolecules 9:57–65. doi:10.1021/bm700769p
Espino-Pérez E, Domenek S, Belgacem N et al (2014) Green process for chemical functionalization of nanocellulose with carboxylic acids. Biomacromolecules 15:4551–4560. doi:10.1021/bm5013458
Eyley S, Thielemans W (2014) Surface modification of cellulose nanocrystals. Nanoscale 6:7764–7779. doi:10.1039/c4nr01756k
French AD (2014) Idealized powder diffraction patterns for cellulose polymorphs. Cellulose 21:885–896. doi:10.1007/s10570-013-0030-4
Fumagalli M, Sanchez F, Boisseau SM, Heux L (2013) Gas-phase esterification of cellulose nanocrystal aerogels for colloidal dispersion in apolar solvents. Soft Matter 9:11309. doi:10.1039/c3sm52062e
Gårdebjer S, Bergstrand A, Idström A et al (2015) Solid-state NMR to quantify surface coverage and chain length of lactic acid modified cellulose nanocrystals, used as fillers in biodegradable composites. Compos Sci Technol 107:1–9. doi:10.1016/j.compscitech.2014.11.014
Habibi Y (2014) Key advances in the chemical modification of nanocelluloses. Chem Soc Rev 43:1519–1542. doi:10.1039/c3cs60204d
Habibi Y, Dufresne A (2008) Highly filled bionanocomposites from functionalized polysaccharide nanocrystals. Biomacromolecules 9:1974–1980. doi:10.1021/bm8001717
Hamad WY, Hu TQ (2010) Structure-process-yield interrelations in nanocrystalline cellulose extraction. Can J Chem Eng. doi:10.1002/cjce.20298
Hansen CM (2007) Hansen solubility parameters a user's handbook, 2nd edn. CRC Press, Boca Raton
Hartig SM (2013) Basic image analysis and manipulation in ImageJ. In: Taylor GP (ed) Current protocols in molecular biology. Wiley, Hoboken, pp 1–12
Hasani M, Cranston ED, Westman G, Gray DG (2008) Cationic surface functionalization of cellulose nanocrystals. Soft Matter 4:2238. doi:10.1039/b806789a
Heinze T, Liebert T, Koschella A (2006) Esterification of polysaccharides. Springer-Verlag, Berlin. doi:10.1007/3-540-32112-8
Herrick FW, Casebier RL, Hamilton KJ, Sandberg KR (1983) Microfibrillated cellulose: morphology and accessibility. J Appl Polym Sci Appl Polym Symp 37:797–813
Heux L, Chauve G, Bonini C (2000) Nonflocculating and chiral-nematic self-ordering of cellulose microcrystals suspensions in nonpolar solvents. Langmuir 16:8210–8212. doi:10.1021/la9913957
Hobbs SK, Monsky WL, Yuan F et al (1998) Regulation of transport pathways in tumor vessels: role of tumor type and microenvironment. Proc Natl Acad Sci USA 95:4607–4612. doi:10.1073/pnas.95.8.4607
Hussain MA, Liebert T, Heinze T (2004) Acylation of cellulose with *N,N′*-carbonyldiimidazole-activated acids in the novel solvent dimethyl sulfoxide/tetrabutylammonium fluoride. Macromol Rapid Commun 25:916–920. doi:10.1002/marc.200300308
Ibbett RN, Domvoglou D, Fasching M (2007) Characterisation of the supramolecular structure of chemically and physically modified regenerated cellulosic fibres by means of high-resolution Carbon-13 solid-state NMR. Polymer (Guildf) 48:1287–1296. doi:10.1016/j.polymer.2006.12.034
Isogai A, Saito T, Fukuzumi H (2011) TEMPO-oxidized cellulose nanofibers. Nanoscale 3:71–85. doi:10.1039/c0nr00583e
Jasmani L, Eyley S, Wallbridge R, Thielemans W (2013) A facile one-pot route to cationic cellulose nanocrystals. Nanoscale 5:10207–10211. doi:10.1039/c3nr03456a
Junior de Menezes A, Siqueira G, Curvelo AAS, Dufresne A (2009) Extrusion and characterization of functionalized cellulose whiskers reinforced polyethylene nanocomposites. Polymer (Guildf) 50:4552–4563. doi:10.1016/j.polymer.2009.07.038
Kim SH, Lee CM, Kafle K (2013) Characterization of crystalline cellulose in biomass: basic principles, applications, and limitations of XRD, NMR, IR, Raman, and SFG. Korean J Chem Eng 30:2127–2141. doi:10.1007/s11814-013-0162-0

Labet M, Thielemans W (2011) Improving the reproducibility of chemical reactions on the surface of cellulose nanocrystals: ROP of ε-caprolactone as a case study. Cellulose 18:607–617. doi:10.1007/s10570-011-9527-x

Labet M, Thielemans W (2012) Citric acid as a benign alternative to metal catalysts for the production of cellulose-grafted-polycaprolactone copolymers. Polym Chem 3:679–684. doi:10.1039/c2py00493c

Lee K-Y, Bismarck A (2012) Susceptibility of never-dried and freeze-dried bacterial cellulose towards esterification with organic acid. Cellulose 19:891–900. doi:10.1007/s10570-012-9680-x

Lee KY, Quero F, Blaker JJ et al (2011) Surface only modification of bacterial cellulose nanofibres with organic acids. Cellulose 18:595–605. doi:10.1007/s10570-011-9525-z

Lin N, Dufresne A (2014) Surface chemistry, morphological analysis and properties of cellulose nanocrystals with gradiented sulfation degrees. Nanoscale 6:5384–5393. doi:10.1039/c3nr06761k

Lin N, Huang J, Chang PR et al (2011) Surface acetylation of cellulose nanocrystal and its reinforcing function in poly(lactic acid). Carbohydr Polym 83:1834–1842. doi:10.1016/j.carbpol.2010.10.047

Liu J-C, Moon RJ, Rudie A, Youngblood JP (2014) Mechanical performance of cellulose nanofibril film-wood flake laminate. Holzforschung 68:283–290. doi:10.1515/hf-2013-0071

Liu J-C, Martin DJ, Moon RJ, Youngblood JP (2015) Enhanced thermal stability of biomedical thermoplastic polyurethane with the addition of cellulose nanocrystals. J Appl Polym Sci 132:41970. doi:10.1002/app.41970

Majoinen J, Walther A, McKee JR et al (2011) Polyelectrolyte brushes grafted from cellulose nanocrystals using Cu-mediated surface-initiated controlled radical polymerization. Biomacromolecules 12:2997–3006. doi:10.1021/bm200613y

Missoum K, Belgacem MN, Barnes J-P et al (2012) Nanofibrillated cellulose surface grafting in ionic liquid. Soft Matter 8:8338–8349. doi:10.1039/c2sm25691f

Missoum K, Belgacem MN, Bras J (2013) Nanofibrillated cellulose surface modification: a review. Materials (Basel) 6:1745–1766. doi:10.3390/ma6051745

Moon RJ, Martini A, Nairn J et al (2011) Cellulose nanomaterials review: structure, properties and nanocomposites. Chem Soc Rev 40:3941–3994. doi:10.1039/c0cs00108b

Morandi G, Heath L, Thielemans W (2009) Cellulose nanocrystals grafted with polystyrene chains through surface-initiated atom transfer radical polymerization (SI-ATRP). Langmuir 25:8280–8286. doi:10.1021/la900452a

Navarro JRG, Conzatti G, Yu Y et al (2015) Multicolor fluorescent labeling of cellulose nanofibrils by click chemistry. Biomacromolecules. doi:10.1021/acs.biomac.5b00083

Newman RH (2004) Homogeneity in cellulose crystallinity between samples of Pinus radiata wood. Holzforschung 58:91–96. doi:10.1515/HF.2004.012

Nielsen LJ, Eyley S, Thielemans W, Aylott JW (2010) Dual fluorescent labelling of cellulose nanocrystals for pH sensing. Chem Commun (Camb) 46:8929–8931. doi:10.1039/c0cc03470c

Park S, Baker JO, Himmel ME et al (2010) Cellulose crystallinity index: measurement techniques and their impact on interpreting cellulase performance. Biotechnol Biofuels 3:10. doi:10.1186/1754-6834-3-10

Peng SX, Moon RJ, Youngblood JP (2014) Design and characterization of cellulose nanocrystal-enhanced epoxy hardeners. Green Mater 2:193–205. doi:10.1680/gmat.14.00015

Podsiadlo P, Choi S-Y, Shim B et al (2005) Molecularly engineered nanocomposites: layer-by-layer assembly of cellulose nanocrystals. Biomacromolecules 6:2914–2918. doi:10.1021/bm050333u

Reiner RS, Rudie AW (2013) Process scale-up of cellulose nanocrystal production to 25 kg per batch at the forest products laboratory. In: Postek MT, Moon RJ, Rudie AW, Bilodeau MA (eds) Production and applications of Cellulose nanomaterials. TAPPI Press, Peachtree Corners, pp 21–24

Reising AB, Moon RJ, Youngblood JP (2012) Effect of particle alignment on mechanical properties of neat cellulose nanocrystal films. J Sci Technol For Prod Process 2:32–41

Rietveld HM (1969) A profile refinement method for nuclear and magnetic structures. J Appl Crystallogr 2:65–71. doi:10.1107/S0021889869006558

Sadeghifar H, Filpponen I, Clarke SP et al (2011) Production of cellulose nanocrystals using hydrobromic acid and click reactions on their surface. J Mater Sci 46:7344–7355. doi:10.1007/s10853-011-5696-0

Sassi JF, Chanzy H (1995) Ultrastructural aspects of the acetylation of cellulose. Cellulose 2:111–127. doi:10.1007/BF00816384

Sèbe G, Ham-Pichavant F, Ibarboure E et al (2012) Supramolecular structure characterization of cellulose II nanowhiskers produced by acid hydrolysis of cellulose I substrates. Biomacromolecules 13:570–578. doi:10.1021/bm201777j

Siqueira G, Bras J, Dufresne A (2009) Cellulose whiskers versus microfibrils: influence of the nature of the nanoparticle and its surface functionalization on the thermal and mechanical properties of nanocomposites. Biomacromolecules 10:425–432. doi:10.1021/bm801193d

Siqueira G, Bras J, Dufresne A (2010) New process of chemical grafting of cellulose nanoparticles with a long chain isocyanate. Langmuir 26:402–411. doi:10.1021/la9028595

Sugiyama J, Vuong R, Chanzy H (1991) Electron-diffraction study on the two crystalline phases occurring in native cellulose from an algal cell-wall. Macromolecules 24:4168–4175. doi:10.1021/ma00014a033

Thielemans W, Belgacem MN, Dufresne A (2006) Starch nanocrystals with large chain surface modifications. Langmuir 22:4804–4810. doi:10.1021/la053394m

Tian C, Fu S, Habibi Y, Lucia LA (2014) Polymerization topochemistry of cellulose nanocrystals: a function of surface dehydration control. Langmuir 30:14670–14679. doi:10.1021/la503990u

Vaca-Garcia C, Borredon ME, Gaseta A (2001) Determination of the degree of substitution (DS) of mixed cellulose esters by elemental analysis. Cellulose 8:225–231. doi:10.1023/A:1013133921626

Xiao L, Mai Y, He F et al (2012) Bio-based green composites with high performance from poly(lactic acid) and surface-modified microcrystalline cellulose. J Mater Chem 22:15732–15739. doi:10.1039/c2jm32373g

Yuan H, Nishiyama Y, Wada M, Kuga S (2006) Surface acylation of cellulose whiskers by drying aqueous emulsion. Biomacromolecules 7:696–700. doi:10.1021/bm050828j

Zhou Y, Fuentes-Hernandez C, Khan TM et al (2013) Recyclable organic solar cells on cellulose nanocrystal substrates. Sci Rep 3:1536. doi:10.1038/srep01536